Latitudinally asymmetric response of global surface temperature: Implications for regional climate change

Yangyang Xu[1] and Veerabhadran Ramanathan[1]

Received 23 April 2012; revised 7 June 2012; accepted 9 June 2012; published 11 July 2012.

[1] The Earth's climate system was subject to two multi-decadal warming trends in the beginning (1910–1940) and end (1975–2005) of the 20th century, having been interrupted only by a cooling trend in mid-century (1940–1975). The spatio-temporal distribution of surface temperature during this time, especially the land-ocean warming contrast in recent decades, has been the subject of many climate change detection studies. The focus of this study is the south-to-north warming asymmetry and we observed a similar Latitudinal Asymmetry of Temperature Change (LATC) for the two warming sub-periods and the cooling sub-period. Basically, the temperature change was low in the Southern Hemisphere extra-tropics (60°S) and increased monotonically to peak values (0.15°C/decade for warming trends) in the Northern Hemisphere extra-tropics (60°N). We hypothesized that the LATC is a fundamental characteristic of the planet's transient response to global forcing. We tested this hypothesis using climate model simulations of CO_2 and aerosol forcing, and the simulations revealed very similar LATC as seen in the observations. In the simulations, the LATC did not depend on the asymmetry of the forcing and furthermore weakened significantly in equilibrium simulations, leading to the deduction that the LATC was caused by a corresponding asymmetry in the land-ocean fraction, i.e., the analyses of model simulations supported the hypothesis of LATC being a fundamental characteristic of the planet's transient response. If LATC is preserved as the planet warms beyond 2°C, precipitation patterns can be drastically disrupted in the tropics and sub-tropics, with major implications for regional climate. **Citation:** Xu, Y., and V. Ramanathan (2012), Latitudinally asymmetric response of global surface temperature: Implications for regional climate change, *Geophys. Res. Lett.*, *39*, L13706, doi:10.1029/2012GL052116.

1. Introduction

[2] As an important indicator of climate change, changes in global surface temperature during the 20th century have been studied extensively [*Trenberth et al.*, 2007]. Some of the earliest detection methods for and signals attributed to global warming began in the 1980s [*Madden and Ramanathan*, 1980], and these gave way to further numerous sophisticated attempts to detect and measure climate changes [*Santer et al.*, 2009]. The focus now is on determining higher order moments–spatial and temporal asymmetries of the warming trend. Numerous studies in which the land-ocean contrast has been examined have clearly established that land-surface warming is larger than the warming of the sea, especially during the rapid warming sub-period prior to the 1970s [*Braganza et al.*, 2003; *Sutton et al.*, 2007; *Trenberth et al.*, 2007; *Joshi et al.*, 2008; *Lambert et al.*, 2011; *Drost et al.*, 2011]. Models are able to simulate this contrast but the contrast shows up both in transient simulations and equilibrium simulations, leading to the conclusion that the larger warming over land is due to surface-atmosphere feedbacks [*Sutton et al.*, 2007; *Joshi et al.*, 2008].

[3] Two other spatial asymmetries examined considered the difference in warming trends between the Northern Hemisphere (NH), Southern Hemisphere (SH) [e.g., *Braganza et al.*, 2003], and latitudinal gradient of the warming within the NH [*Gitelman et al.*, 1997]. Many studies have shown that the NH warming is much larger than that in the SH [e.g., *Drost et al.*, 2011]. Furthermore, within the NH, polar latitudes had larger warming than the lower latitudes, thus weakening the latitudinal temperature gradient [*Drost et al.*, 2011] within the NH. In order to factor in all above-mentioned asymmetries in the warming trend, *Drost et al.* [2011] proposed six indices that included global mean temperature as well as the difference in land-ocean and NH-SH warmings. In summary, past work has well established that the NH latitudinal temperature gradient is weakening, and there is asymmetry in the warming trend between the NH and the SH. From attempts to understand this asymmetry using model simulations [*Braganza et al.*, 2003; *Stott et al.*, 2006; *Drost et al.*, 2011] it is inferred that the NH-SH asymmetric trend is indicative of anthropogenic influences in the global mean trend.

[4] This study, which was built on earlier studies, identifies a new metric for the NH-SH asymmetry in terms of a normalized latitudinal temperature gradient. Also included is a detailed analysis of the underlying causal factor for the asymmetry. Our study of 20th century trends of latitudinal temperature gradients also differentiates from earlier studies in the following ways: a) We considered trends from 60°S to 60°N and not only in the NH. Earlier studies [*Gitelman et al.*, 1997; *Braganza et al.*, 2003; *Drost et al.*, 2011] were limited to 50–55°N and 30–35°N. b) Whereas earlier studies focused on century time scale trends, we divided the 20th century into three sub-periods: early warming sub-period from 1910 to 1940, middle cooling sub-period from 1940 to 1975, and late warming sub-period from 1975 to 2005. This new approach enabled us to identify a characteristic pattern of asymmetry in the latitudinal temperature trend that is similar for all three sub-periods, in spite of the significant differences in the global mean trends between the three sub-periods (analysis presented in next section). Based on the empirical data, we hypothesized that this characteristic pattern of asymmetry is

[1]Scripps Institution of Oceanography, University of California, San Diego, La Jolla, California, USA.

Corresponding author: Y. Xu, Scripps Institution of Oceanography, University of California, San Diego, La Jolla, CA 92013, USA. (yangyang@ucsd.edu)

0094-8276/12/2012GL052116

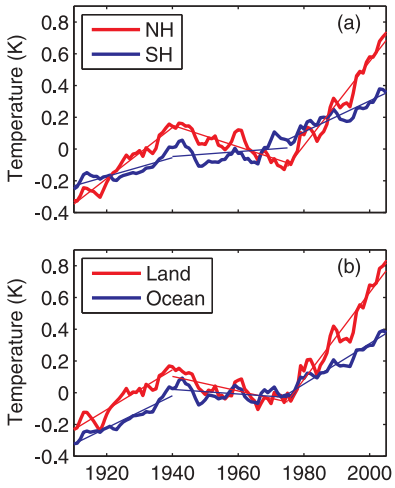

Figure 1. Observed temperature changes (1910–2005) for (a) NH and SH and (b) land and ocean. Temperature is shown as an anomaly relative to the base period 1951–1980. Linear fits of temperature trends (thin lines) made for the three sub-periods illustrate multi-decadal temperature variations (1910–1940, 1940–1975, 1975–2005). The sub-period intervals were chosen based on multi-decadal global mean trends [*Trenberth*, 1990]. Using this approach also avoided incorporating years containing questionable measurements [*Thompson et al.*, 2008, 2010] as starting or ending points.

caused by the corresponding latitudinal asymmetry in the land-ocean fraction. We tested this hypothesis with available 3-D climate model simulations. In the final section, we explored the implication of asymmetric trends for regional precipitation changes.

2. Surface Temperature Change in the 20th Century: Latitudinal Asymmetry

[5] Before examining latitudinal asymmetry, we first revisit the pattern of global and hemispherical mean temperature trends from the gridded temperature record compiled by the Goddard Institute for Space Studies [*Hansen et al.*, 2010]. Revisiting this issue was necessary because other published studies dealt largely with the 20th century as a whole or only the last half of the century. Here, we considered three sub-periods based on the NH experiencing a 0.48 ± 0.13°C (95% confidence interval) warming during the first three decades ending in the 1940s, then shifting to a cooling of −0.24 ± 0.12°C from 1940 to 1975, which was followed by a large warming of 0.8 ± 0.16°C from 1975 to 2005 (Figure 1a). The SH did not demonstrate a statistically significant mid-century cooling (Figure 1a), and the 1975–2005 warming was only 0.3 ± 0.11°C lower than the NH trend by a factor of 2.5. The hemispherical and global mean values in Figure S1 and Table S1 in the auxiliary material show the entire trend analyses for reference.[1] Another well-known feature from earlier studies highlights the trend's land-ocean contrast (Figure 1b). Multi-decadal trends were more pronounced over the land surface, with warming of 0.38 ± 0.15°C, cooling of −0.16 ± 0.14°C, and then warming of 0.82 ± 0.2°C, respectively, during the three sub-periods. In contrast, the ocean surface experienced two smaller warming (0.3°C and 0.38°C) trends in the beginning and end of the century, while the mid-century trend was not significant (−0.05 ± 0.1°C). Analyses separating the NH mean temperature into a land and ocean component (Figure S1) show that the NH land experienced larger trends compared with the NH ocean (e.g., two times the larger warming during the last sub-period), making it the strongest contributor to the warming-cooling-warming pattern observed in global average temperature trends. As to the underlying message, a time-series analysis of 20th century surface temperatures must account for multi-decadal changes in the sign and magnitude of the trends. The analysis above was performed with data from 60°S to 60°N, excluding Polar Regions. We limited the analysis to this latitude band because it avoids the less reliable observations from the Arctic regions [*Chylek et al.*, 2009], particularly for the 1910–1940 sub-period [e.g., see *Gitelman et al.*, 1997]. In addition, the Antarctic continent's higher elevation makes it difficult to estimate a gradient in surface temperature from sea level to the elevated continent. However, we found that the main features of the hemispheric multi-decadal variations also appear if analysis is carried out with temperature data from 90°S to 90°N (Figure S1).

[6] We determined that temperature trends separately as a function of latitude for the three sub-periods. Focusing first on the two sub-periods subject to strong warming (1910–1940 and 1975–2005), the trends over the ocean were relatively small in the SH extra-tropics (Figure 2a) and increased northward with a maximum of about 0.25–0.35°C /decade in the NH extra-tropics. The mid-century cooling sub-period also showed a similar pattern of maximum change in the NH extra-tropics. We illustrated the latitudinal gradient of oceanic temperature trends in Figure 2b (slope of linear fits). It should be noted that, to better display the similarity in the latitudinal asymmetry, the trend in 1940–1975 (negative) was reversed in sign and adjusted with an offset of 0.1°C. This offset does not affect the asymmetric feature or the latitudinal gradient. The trend's latitudinal gradient for 1940–1975 (blue curve) is 0.0012°C /decade/degree (95% confidence interval ranging from 0.0009 to 0.0016, as shown by color shading). The other two linear fits (0.0009 for 1910–1940 and 0.0018 for 1975–2005) are nearly within the 95% confidence interval. The factor-of-two difference in the gradient between the two warming sub-periods reduced to a factor of about 1.5 when the trends were normalized with the respective global mean (60°S to 60°N) warming trends (Figure 2c). Normalized trends are also compared in the next section due to large differences in trends between observations and various simulations.

[7] In summary, irrespective of the differences in the magnitudes and signs of the three observed trends, their latitudinal asymmetries were statistically similar. Thus, the asymmetry of temperature trends (see Figure S2 for land) is possibly a fundamental characteristic of the response of the climate system to global forcing.

3. Understanding Latitudinal Asymmetry

[8] The fundamental causal factors for similarity in the latitudinal asymmetry of temperature trend are explored using simulations from a Global Climate Model (GCM)

[1]Auxiliary materials are available in the HTML. doi:10.1029/2012GL052116.

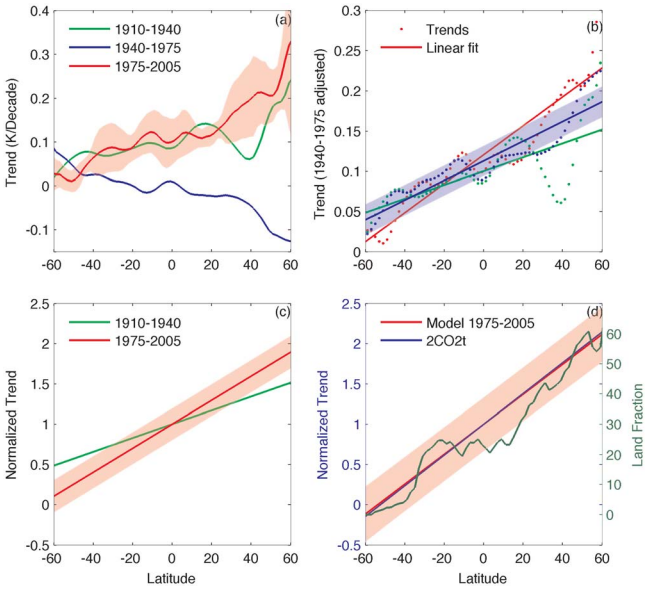

Figure 2. Latitudinal asymmetry of temperature trends for the ocean. (a) Warming trends (°C/decade) of surface ocean temperature for the three sub-periods of the 20th century, as a function of latitude (60°S–60°N). Trends were calculated based on a linear fit method shown in Figure 1. Uncertainty in the warming trend for one sub-period is shown in shading area. (b) Temperature trends (color dots) are the same as for Figure 2a, except the 1940–1975 trends were reversed in sign and adjusted with 0.1°C. The latitudinal gradient is shown with linear fits (solid lines). Uncertainty of linear fits is shown in shaded color. (c) Latitudinal gradients of normalized trends (relative to global average) for 1910–1940 and 1975–2005 warming sub-periods. (d) Latitudinal gradient of normalized trends (relative to global average) in the GFDL model resulted under two different simulations (1975–2005 in the 20th century simulation, CO_2-doubling transient simulation or $2CO_2t$). Surface temperatures from GFDL and MPI model outputs were obtained from the World Climate Research Program's Coupled Model Inter-comparison Project phase 3 (CMIP3) multi-model dataset [*Meehl et al.*, 2007]. Temperature change for the transient phase (year 10–40) and for the quasi-equilibrium phase (year 190–220) were calculated by differencing a 30-year average temperature with the average temperature in the corresponding sub-periods from a control simulation.

developed at the Geophysical Fluid Dynamics Laboratory (GFDL-CM2.1 [*Delworth et al.*, 2006]). The 20th century simulation output was used to calculate trends for the three sub-periods following our approach for the observational record. The 20th century simulation adopted time-varying anthropogenic greenhouse gases and aerosol forcing, as well as changes in natural forcing such as incident solar radiation and volcanic aerosols. Trends simulated by the model (Figure S3a) were generally consistent with observed trends (Figure 2a). The asymmetry of the normalized trend for the last sub-period had a gradient of 0.019 (0.015–0.024) deg^{-1} (Figure 2d) and was consistent with the observed asymmetry of 0.015 (0.012–0.018) (Figure 2c). One confounding issue with the 20th century simulation was the inclusion of aerosol forcing, which had strong inter-hemispheric asymmetry and, thus, could influence temperature trend asymmetry. To eliminate this possibility, we redid the analysis with the GFDL-CM2.1 output for the so-called CO_2-doubling simulation. For this simulation, the CO_2 concentration was initiated at 280 ppm for year 1 and was increased 1% per year until it reached 560 ppm at year 70. The CO_2 concentration was fixed at 560 ppm, and the model continued to run for another 180 years. The temperature change during the transient phase (defined as $2CO_2t$) was calculated for year 15–45 by comparison with another control simulation in which the CO_2 concentration was fixed at 280 ppm. The normalized temperature increase for the transient phase yet again demonstrated a pattern of south-to-north asymmetry that was similar to that for the 20th century simulation (Figure 2d). The analyses were repeated with output from the MPI GCM (ECHAM5/MPI-OM) [*Jungclaus et al.*, 2006]. Even though the MPI model yielded a different absolute value of temperature trends for the three sub-periods, the south-to-north asymmetry pattern was similar (Figure S4). Note that the two GCM simulations utilized different CO_2 and aerosol forcings for the 20th century simulation, while the CO_2-doubling simulation used only CO_2 forcing. Despite diverse forcing magnitudes, latitudinal asymmetry in the temperature response was preserved in both models. The fundamental inference was the asymmetry pattern of normalized temperature trend with a gradient of 0.015–0.019 $degree^{-1}$, which was a model-independent characteristic.

[9] From these model simulations, we concluded that the observed latitudinal asymmetry was independent of the asymmetry from forcing; hence, forcing was not a causal factor for the asymmetry. The only logical deduction is that the asymmetry was due to a corresponding latitudinal asymmetry in the landmass fraction, which increased monotonically from 0% at 60°S to 70% at 60°N (Figure 2d). Why then did the latitude band with the larger land fraction exhibit larger temperature trends? Studies have shown two potential contributing factors to the larger warming seen over land compared to that over the ocean at the same latitude [*Lambert et al.*, 2011]. First, the ocean has a much larger heat capacity than does land. Second, a model has shown [*Sutton et al.*, 2007] that in response to the same forcing, equilibrium temperature changes over land are larger than those over the ocean due to stronger negative evaporation feedbacks over the sea surface [*Manabe et al.*, 1991]. Because of the climate system's fixed land-ocean area, the cumulative effect of the land-ocean warming contrast was mapped onto a pattern of south-to-north asymmetry in temperature trends, both over land and over the ocean. The analysis was also extended to include Arctic region up to 90°N in Figure S5, and the same asymmetric feature is reproduced. However, we note that the amplified warming over Arctic can also be potentially contributed by sea ice feedback mechanism, which is beyond the scope of our discussion.

[10] One way to verify the above conclusion was to examine temperature changes for the equilibrium state, which should exhibit a weaker asymmetry because the factor dealing with the ocean's heat capacity would not play a role. The temperature change in a quasi-equilibrium state ($2CO_2e$, year 190–220, 120 years after CO_2 was doubled) was calculated by comparison to a control simulation (280 ppm CO_2 fixed). As shown in Figure S3c (see $2CO_2e$), the asymmetry is less than 0.008 deg^{-1} compared with 0.019 deg^{-1} for

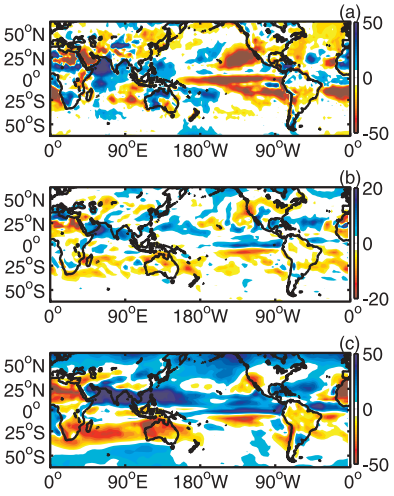

Figure 3. Precipitation rate changes (%). (a) 1979–2009 observations. The absolute precipitation change was determined from linear fits of a 30-year long time-series at each grid. The percentage of change was the absolute change divided by the long-term mean. (b) Simulated changes in the experiment (SST_Grd) in which the SST gradient was imposed with global mean increase of 0.3°C. (c) Simulated changes in the experiment (SST_GrdLarge) in which SST gradient was imposed with global mean increase of 2.5°C. The percentage of simulated change was determined by comparison with a control experiment incorporating climatologic SST. Areas with small changes were considered statistically insignificant and thus left white. Observed precipitation was obtained from Global Precipitation Climatology Project (GPCP version 2.1 [*Adler et al.*, 2003]). Precipitation trends were calculated using the method adopted for temperature observation.

the transient case ($2CO_2$t curve). The asymmetry did not completely diminish because (1) 120 years is not long enough for the coupled ocean-atmosphere system to reach a true equilibrium state, and (2) even if equilibrium was reached, for the same forcing, the warming over land is larger than that of the ocean due to less climate sensitivity over the ocean.

[11] Our finding that the latitudinal asymmetry is governed by latitudinal variations in land and ocean fraction is intuitive and could have been inferred from earlier studies [e.g., *Drost et al.*, 2011]. Yet our study is unique in demonstrating this fundamental feature of transient warming and in using a combination of observations and model simulations to establish its causal factor. In particular, (1) by subdividing the 20th century trend into three subperiods, we have shown that the asymmetric response is statistically similar for all periods (Figure 2b) irrespective of the forcing being different and the global mean trend being different in both magnitude and sign. This near similarity provides compelling proof that the latitudinal gradient is a fundamental characteristic of the climate system response to global forcing. (2) By comparing the latitudinal gradient ($0.015\ \mathrm{deg}^{-1}$) of the normalized temperature trend in the last sub-period from observing (Figure 2c) model simulations of the 20th century (with aerosol + CO_2 forcing) and with CO_2 forcing only (Figure 2d), we have shown that the simulated gradient of $0.019\ \mathrm{deg}^{-1}$ not only compares well with the observed value of $0.015\ \mathrm{deg}^{-1}$ but is also independent of the spatial patterns of the forcing. (3) Finally, the gradient of normalized temperature trend decreased significantly from $0.019\ \mathrm{deg}^{-1}$ in CO_2-doubling transient simulations to less than $0.008\ \mathrm{deg}^{-1}$ in equilibrium simulations. This factor-of-two decrease in the gradient further confirmed that asymmetry in the normalized temperature trends was driven by corresponding asymmetry in the land-ocean fraction.

4. Implications for Regional Climate Changes: Present and Future

[12] The latitudinal asymmetry of temperature response is likely to be a zeroth-order approximation of global warming spatial pattern in the 21st century. An important consequence is the potential impact on regional precipitation response, a topic receiving increasing attention [*Held et al.*, 2005; *Chung and Ramanathan*, 2006; *Xie et al.*, 2010; *Vecchi et al.*, 2011]. We conducted idealized GCM experiments with a zonally uniform SST latitudinal gradient to illustrate the impact of latitudinal asymmetry of ocean warming. We used the National Center for Atmospheric Research (NCAR) CESM1.0 model [*Gent et al.*, 2011] to simulate a global climate response to two distinctly different patterns of sea surface temperature (SST) increases from a climatological SST pattern. The first imposed a uniform SST increase of 0.3°C everywhere in the model domain (SST_Uniform). The second imposed a linear gradient of SST increase (SST_Grd) ranging from 0°C at 60°S to 0.6°C at 60°N with a global mean increase of 0.3°C to mimic the observed trends during 1975–2005. The control run prescribed observed sea surface temperature (SST_control). CESM simulations were run for 35 years in a resolution of 2.8° × 2.8°. The first 5 years was for spinning up, and the remaining 30 years enabled us to obtain a statistically significant long-term temperature and precipitation average. The simulated precipitation changes in the asymmetric SST warming experiment (SST_Grd, Figure 3b) showed an increase in northern tropical precipitation. A particularly strong precipitation increase (20%) over the Northern Indian Ocean illustrated the strong sensitivity of the Indian monsoon to changes in the SST gradient [*Chung and Ramanathan*, 2006], which was also seen in the observed trend. Simulated precipitation over many parts of the Southern tropics and Western North America decreased by about 10%, and these features were also seen in the observed trend. However, the observed negative trend was much stronger. A one-to-one comparison across the globe was not warranted, since the simulation ignored the important effects of aerosol forcing on regional precipitation [*Rotstayn and Lohmann*, 2002] and the detailed spatial pattern of SST change over past decades.

[13] One major implication of these results is that the planet's future transient warming will continue to be subject to the south-to-north asymmetry (Figure 2d), meaning the impact of the asymmetric response is likely to grow with time. Even if CO_2 concentration is stabilized at current levels, the committed warming due to current GHG forcing [*Wigley*, 2005; *Ramanathan and Feng*, 2008] would be as much as 2.5°C compared with preindustrial era. To explore the implications of a larger warming accompanied by the asymmetric pattern, we performed another model simulation (SST_GrdLarge) in which the imposed warming had a south-to-north asymmetry similar to the gradient in Figure 2b but

with a global mean sea surface warming of 2.5°C. Results showed a similar pattern to that from the SST_Grd simulation but the change was larger in magnitude by a factor of 5–10 (Figure 3c). Africa, Western North America, the Amazon region of South America, and Australia were subject to intense droughts of up to a 50% decline in precipitation. The droughts simulated in these regions were accompanied by a large increase (50%) in Indian monsoon rainfall. Shifts in regional precipitation patterns shown in Figure 3c would pose enormous challenges for the ecosystem and the populations living in the tropical and sub-tropical regions. Since the models (at least the ones used in this study) accounted for latitudinal asymmetry, in principle, their simulations for the 21st century should simulate the large precipitation shifts shown in Figure 3c. However, given the enormous difficulty in interpreting model results, findings here can guide the interpretation of model simulations for the future.

[14] **Acknowledgments.** We thank the two anonymous reviewers for their insightful comments on the paper, which immensely helped in improving the clarity of the presentation. The study was supported by the National Science Foundation (ATM07-21142). We also acknowledge NCAR's Computational and Information Systems Laboratory for providing computing resources.

[15] The Editor thanks the anonymous reviewer for assisting in the evaluation of this paper.

References

Adler, R. F., et al. (2003), The Version-2 Global Precipitation Climatology Project (GPCP) monthly precipitation analysis (1979–present), *J. Hydrometeorol.*, *4*, 1147–1167, doi:10.1175/1525-7541(2003)004<1147:TVGPCP>2.0.CO;2.

Braganza, K., et al. (2003), Simple indices of global climate variability and change: Part I—Variability and correlation structure, *Clim. Dyn.*, *20*, 491–502.

Chung, C. E., and V. Ramanathan (2006), Weakening of north Indian SST gradients and the monsoon rainfall in India and the Sahel, *J. Clim.*, *19*, 2036–2045, doi:10.1175/JCLI3820.1.

Chylek, P., C. K. Folland, G. Lesins, M. K. Dubey, and M. Wang (2009), Arctic air temperature change amplification and the Atlantic Multidecadal Oscillation, *Geophys. Res. Lett.*, *36*, L14801, doi:10.1029/2009GL038777.

Delworth, T. L., et al. (2006), GFDL's CM2 global coupled climate models. Part I: Formulation and simulation characteristics, *J. Clim.*, *19*, 643–674, doi:10.1175/JCLI3629.1.

Drost, et al. (2011), Communicating global climate change using simple indices: An update, *Clim. Dyn.*, doi:10.1007/s00382-011-1227-6.

Gent, P. R., et al. (2011), The Community Climate System Model Version 4, *J. Clim.*, *24*, 4973–4991, doi:10.1175/2011JCLI4083.1.

Gitelman, A., J. Risbey, R. Kass, and R. Rosen (1997), Trends in the surface meridional temperature gradient, *Geophys. Res. Lett.*, *24*, 1243–1246, doi:10.1029/97GL01154.

Hansen, J., R. Ruedy, M. Sato, and K. Lo (2010), Global surface temperature change, *Rev. Geophys.*, *48*, RG4004, doi:10.1029/2010RG000345.

Held, I. M., et al. (2005), Simulation of Sahel drought in the 20th and 21st centuries, *Proc. Natl. Acad. Sci. U. S. A.*, *102*, 17,891–17,896, doi:10.1073/pnas.0509057102.

Joshi, M. M., et al. (2008), Mechanisms for the land/sea warming contrast exhibited by simulations of climate change, *Clim. Dyn.*, *30*(5), 455–465, doi:10.1007/s00382-007-0306-1.

Jungclaus, J. H., et al. (2006), Ocean circulation and tropical variability in the coupled model ECHAM5/MPI-OM, *J. Clim.*, *19*, 3952, doi:10.1175/JCLI3827.1.

Lambert, F. H., M. J. Webb, and M. M. Joshi (2011), The relationship between land–ocean surface temperature contrast and radiative forcing, *J. Clim.*, *24*, 3239–3256, doi:10.1175/2011JCLI3893.1.

Madden, R. A., and V. Ramanathan (1980), Detecting climate change due to increasing CO_2 in the atmosphere, *Science*, *209*, 763–768, doi:10.1126/science.209.4458.763.

Manabe, S., et al. (1991), Transient responses of a coupled ocean-atmosphere model to gradual changes of atmospheric CO_2, *J. Clim.*, *4*, 785–818, doi:10.1175/1520-0442(1991)004<0785:TROACO>2.0.CO;2.

Meehl, G., et al. (2007), THE WCRP CMIP3 multimodel dataset: A new era in climate change research, *Bull. Am. Meteorol. Soc.*, *88*, 1383, doi:10.1175/BAMS-88-9-1383.

Ramanathan, V., and Y. Feng (2008), On avoiding dangerous anthropogenic interference with the climate system: Formidable challenges ahead, *Proc. Natl. Acad. Sci. U. S. A.*, *105*, 14,245–14,250, doi:10.1073/pnas.0803838105.

Rotstayn, L. D., and U. Lohmann (2002), Tropical rainfall trends and the indirect aerosol effect, *J. Clim.*, *15*, 2103–2116, doi:10.1175/1520-0442(2002)015<2103:TRTATI>2.0.CO;2.

Santer, B. D., et al. (2009), Incorporating model quality information in climate change detection and attribution studies, *Proc. Natl. Acad. Sci. U. S. A.*, *106*, 14,778–14,783, doi:10.1073/pnas.0901736106.

Stott, P., et al. (2006), Observational constraints on past attributable warming and predictions of future global warming, *J. Clim.*, *19*, 3055–3069, doi:10.1175/JCLI3802.1.

Sutton, R. T., B. Dong, and J. M. Gregory (2007), Land/sea warming ratio in response to climate change: IPCC AR4 model results and comparison with observations, *Geophys. Res. Lett.*, *34*, L02701, doi:10.1029/2006GL028164.

Thompson, D. W. J., et al. (2008), A large discontinuity in the mid-twentieth century in observed global-mean surface temperature, *Nature*, *453*, 646–649, doi:10.1038/nature06982.

Thompson, D. W. J., et al. (2010), An abrupt drop in Northern Hemisphere sea surface temperature around 1970, *Nature*, *467*, 444–447, doi:10.1038/nature09394.

Trenberth, K. E. (1990), Recent observed interdecadal climate changes in the Northern Hemisphere, *Bull. Am. Meteorol. Soc.*, *71*, 988–993, doi:10.1175/1520-0477(1990)071<0988:ROICCI>2.0.CO;2.

Trenberth, K. E. et al. (2007), Observations: Surface and atmospheric climate change, in *Climate Change 2007: The Physical Science Basis. Contribution of Working Group I to the Fourth Assessment Report of the Intergovernmental Panel on Climate Change*, edited by S. Solomon et al., pp. 235–336, Cambridge Univ. Press, Cambridge, U. K.

Vecchi, G., et al. (2011), Statistical-dynamical predictions of seasonal North Atlantic hurricane activity, *Mon. Weather Rev.*, *139*, 1070–1082, doi:10.1175/2010MWR3499.1.

Wigley, T. M. L. (2005), The climate change commitment, *Science*, *307*, 1766–1769, doi:10.1126/science.1103934.

Xie, S.-P., et al. (2010), Global warming pattern formation: Sea surface temperature and rainfall, *J. Clim.*, *23*, 966–986, doi:10.1175/2009JCLI3329.1.